Laser and Particle Beams (2017), *35*, 159–169.
© Cambridge University Press, 2017 0263-0346/17
doi:10.1017/S0263034617000039

Magnetic field effect on laser-induced breakdown spectroscopy and surface modifications of germanium at various fluences

H. IFTIKHAR, S. BASHIR, A. DAWOOD, M. AKRAM, A. HAYAT, K. MAHMOOD, A. ZAHEER, S. AMIN, AND F. MURTAZA

Centre for Advanced Studies in Physics (CASP), Government College University (GCU), Lahore, Pakistan

(RECEIVED 8 November 2016; ACCEPTED 8 January 2017)

Abstract

The effect of the transverse magnetic field on laser-induced breakdown spectroscopy and surface modifications of germanium (Ge) has been investigated at various fluences. Ge targets were exposed to Nd: YAG laser pulses (1064 nm, 10 ns, 1 Hz) at different fluences ranging from 3 to 25.6 J/cm^2 to generate Ge plasma under argon environment at a pressure of 50 Torr. The magnetic field of strength 0.45 Tesla perpendicular to the direction of plasma expansion was employed by using two permanent magnets. The emission spectra of laser-induced Ge plasma was detected by the laser-induced breakdown spectroscopy system. The electron temperature and number density of Ge plasma are evaluated by using the Boltzmann plot and stark broadening methods, respectively. The variations in emission intensity, electron temperature (T_e), and number density (n_e) of Germanium plasma are explored at various fluences, with and without employment of the magnetic field. It is observed that the magnetic field is responsible for significant enhancement of both excitation temperature and number density at all fluences. It is revealed that an excitation temperature increases from $T_{e,max,without\ B} = 16{,}190$ to $T_{e,max,with\ B} = 20{,}123$ K. Similarly, the two times enhancement in the electron density is observed from $n_{e,max,without\ B} = 2 \times 10^{18}$ to $n_{e,max,with\ B} = 4 \times 10^{18}$ cm^{-3}. The overall enhancement in Ge plasma parameters in the presence of the magnetic field is attributed to the Joule heating effect and adiabatic compression. With increasing fluence both plasma parameters increase and achieve their maxima at a fluence of 12.8 J/cm^2 and then decrease. In order to correlate the plasma parameters with surface modification, scanning electron microscope analysis of irradiated Ge was performed. Droplets and cones are formed for both cases. However, the growth of ridges and distinctness of features is more pronounced in case of the absence of the magnetic field; whereas surface structures become more diffusive in the presence of the magnetic field.

Keywords: Laser-induced breakdown spectroscopy; Electron temperature; Number density; Magnetic confinement; Surface structuring

1. INTRODUCTION

Laser-induced breakdown spectroscopy (LIBS) is an emerging technique, which is widely used to study emission spectra of different materials gases, liquids, and solids (metals, semiconductors, and insulators) (Rai *et al*., 2003*a*, *b*; Michel *et al*., 2007). For simultaneous measurement of aerosol size distribution (Hahn & Lunden, 2000), total mass concentration (Shen *et al*., 2006), species composition (Harilal *et al*., 1998*a*, *b*), detection of radioactive elements, and analysis of trace elements, LIBS is successfully demonstrated as simple, *in situ*, and real-time diagnostic technique (Rai *et al*., 2003*a*, *b*). For evaluating electron temperature and number density of laser-induced plasma, LIBS is also a valuable technique (Farid *et al*., 2011). There are various factors which have a key role in laser-induced plasma formation. These factors include laser parameters (fluence, pulse duration, delay time, and wavelength), material properties, nature, and pressure of environmental gases as well as spatial and temporal confinement techniques (Guo *et al*., 2011; El-Saeid *et al*., 2016).

The plasma confinement by applying the magnetic field is one of the flexible, simple, and cost-effective method. In recent years, magnetically confined plasma has attracted more interest due to its vast ranging applications in inertial

Address correspondence and reprint requests to: S. Bashir, Centre for Advanced Studies in Physics (CASP), Government College University (GCU), Lahore, Pakistan. E-mail: shaziabashir@gcu.edu.pk

https://doi.org/10.1017/S0263034617000039 Published online by Cambridge University Press

confinement fusion (Behera *et al*., 2015), ion implantation (Ahmad *et al*., 2014), pulse laser deposition of thin films (Lan *et al*., 2015), laser propulsion of space vehicles (Burger *et al*., 2016), and tokamaks (Shen *et al*., 2006; Raju *et al*., 2014). The applied magnetic field can be used to control energy and density of plasma species as well as for micro/nanostructuring of materials. Dynamical properties of plasma are significantly influenced by the magnetic field (Behera *et al*., 2015). Due to enhanced confinement and collimation, the stability of plasma can be easily controlled (Harilal *et al*., 2004).

Various groups have investigated the interaction of expanding plasma with the magnetic field (Pisarczyc & Kasperczuk, 1999; Rai *et al*., 2003*a*, *b*). Roy *et al*. (2015) studied collimation of laser-produced plasma using the axial magnetic field. Plasma plume was generated by using Nd:YAG laser pulses. They found that calculated electron temperature and number density showed significant changes in the presence and absence of the magnetic field. The electron temperature increased in the presence of a magnetic field, while number density decreased. Rafique *et al*. (2008) reported that emission intensity is enhanced in the presence of the transverse magnetic field. The main reason for this enhancement is the increased rate of recombination due to high density as a result of confinement. Behera *et al*. (2015) studied the confinement and re-expansion of laser-induced plasma in the transverse magnetic field. Dynamics of a laser-produced carbon plasma expanding in the non-uniform magnetic field is reported by Neogi and Thareja (1999).

The present work is the extension of our previous work in which we have investigated the effect of the magnetic field of strength 0.5 Tesla on Graphite plasma (Arshad *et al*., 2016). The present work deals with investigation of the confinement effect on germanium (Ge) plasma at the magnetic field of strength 0.45 Tesla. The variations in emission intensity, electron temperature and number density of Ge plasma in the presence and absence of the magnetic field at various laser fluences ranging from 3.2 to 25.6 J/cm^2 are investigated. The Germanium plasma was generated in the presence of argon (Ar) gas at a pressure of 50 Torr. The emission intensities are detected by LIBS spectrometer system. The excitation temperature is measured by the Boltzmann distribution method, whereas electron density is evaluated by the stark broadening mechanism. According to our best knowledge no work is reported in which the effect of 0.45 Tesla magnetic field on Ge plasma is investigated at described laser fluences in the presence of Ar environment. The aim of the present work is to explore the effect of the magnetic field on the plasma parameters and surface modifications of Ge plasma. In order to confirm the phenomenon of magnetc field confinement effects on Ge plasma, the targets of Ge were exposed at various fluences ranging from 3.2 to 25.6 J/cm^2 at a fixed Ar gas pressure. With increasing energy deposition, the mass ablation rate increases and correspondingly both T_e and n_e are increased. With further increase in fluence, various phenomenon of saturation and shielding effect take place and no change or decrease in T_e and n_e is observed. However, due to the magnetic field effect, significant increase in T_e and n_e is attributed to confinement effects. The spatial confinement effects, gas dynamical effects, enhancement of collisional frequency of plasma species, and thermal energy coupling can enhance the plasma temperature and charge density. This magnetically confined plasma at optimum pressure and fluence will be highly useful for thin-film deposition, ion implantation as well as inertial confinement fusion. The surface modifications of laser-irradiated Ge are revealed by the scanning electron microscope (SEM) analysis. The purpose of this study is to investigate the effect of the magnetic field under different fluences on micro/nanostrcuturing of Ge.

2. EXPERIMENTAL DETAILS

The schematic of the experimental arrangement used for the laser-induced breakdown spectroscopic analysis of the Ge plasma is shown in Figure 1. Experiments were carried out using fundamental harmonic of Q-Switched Nd: YAG laser 1064 nm (CRF 200: Big Sky laser Technologies, Quantral, France) with pulse duration of 10 ns, repetition rate of 10 Hz, and pulse energy ranging from 25 to 200 mJ. Commercially polished Ge single-crystal (100) samples with dimensions of $10 \times 10 \times 1$ mm^3 were cleaned ultrasonically. Targets were mounted on a target holder in an evacuated multi-port stainless steel chamber. Two permanent magnets (Neodium) each with diameter of 2.54 cm were used to produce the transverse magnetic field. These magnets were mounted and fixed with a holder in parallel to each other on a stainless steel metallic base, placed at the base of the chamber. The distance between the magnets was kept constant, that is, 12 cm. The magnetic field was measured by Gauss meter (GM 08) exactly at the center of two magnets and it comes out to be 0.45 Tesla. Targets were held on the

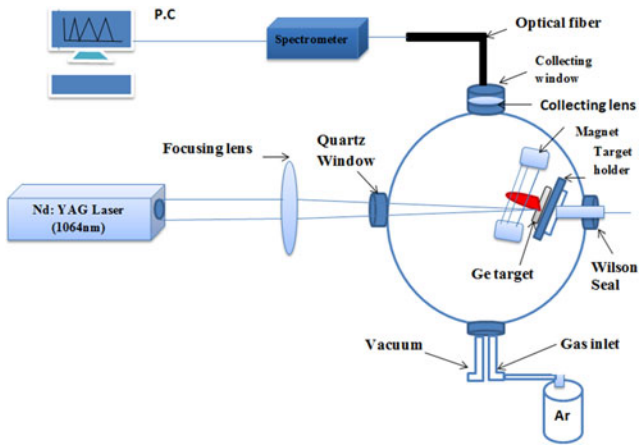

Fig. 1. The schematic representation of experimental setup for investigation of magnetic field effect on laser-induced breakdown spectroscopy and surface modifications of Ge.

https://doi.org/10.1017/S0263034617000039 Published online by Cambridge University Press

target holder in such a way that it was at equal distance from both magnets. The chamber was evacuated to base pressure of 10^{-3} Torr by using rotary pump. The Ar gas was filled in the chamber at a pressure of 50 Torr, which was measured by precisionable pressure gauge. The laser beam was made incident at an angle of 90° w.r.t target surface after passing through focussing lens of focal length 50 cm and Quartz window incorpaorated at one port of the chamber. The focused spot size was 722 μm, which was measured by the SEM analysis. The laser beam generates laser pulses of pulse energy ranging from 25 to 200 mJ, which was controlled by Q-switched delay. The pulsed energy of laser beam was measured by power meter/energy meter (Ophir model 300). In order to avoid the breakdown in environmental gas of Ar, the target was placed before focus, that is, at a distance of 49.8 cm from focusing lens.

The spectra were collected by the LIBS spectrometer system (LIBS 2500 plus) with spectral range of 200–980 nm and a resolution of 0.1 nm. The intensity of emission spectra was enhanced after focusing through collecting lens of focal length 5 cm and it was transmitted through optical fiber to CCD arrays. The OLIBS software was used to analyze the data.

Four sets of experiments were performed.

1. First set of the experiment deals with laser-induced breakdown spectroscopy of Ge plasma in the absence of the magnetic field. In order to investigate the effect of laser fluence, the pulse energy of laser beam was varied from 25, 50, 75, 100, 125, 150 upto 200 mJ corresponding to eight laser fluences of 3, 6.4, 9, 12.8, 16, 19.2, 22, and 25.6 J/cm^2. The experiment was performed in the presence of Ar gas at a pressure of 50 Torr. All other parameters such as distance of target from the focus position, that is, 2 mm and delay time 1.25 μs were kept constant for all measurements.
2. Second set of the experiment deals with the collection of data by LIBS in the presence of the magnetic field by keeping all other parameters fixed. The emission spectra of the laser-induced Ge plasma was collected at various fluences. The same eight set of fluences are used as has been described for set 1.
3. For the SEM analysis the third set of experiment was performed by exposing Ge samples to 50 laser pulses without applying the magnetic field under Ar gas at a pressure of 50 Torr at four different fluences of 6.4, 12.8, 19.2, and 25.6 J/cm^2.
4. In the fourth set of experiment for the SEM analysis, samples were exposed to 50 laser pulses at four same fluences as has been described for set 3. But these exposures were performed in the presence of the magnetic field.

The surface morphology of irradiated Ge targets was investigated by the SEM (JEOL-JSM-6480LV).

3. RESULTS

3.1. Magnetic field effect on LIBS of Ge plasma

3.1.1. Emission intensity

Figure 2 shows the LIBS spectra of Ge plasma obtained at a fluence 16 J/cm^2 in Ar gas at 50 Torr pressure, in the absence and presence of a magnetic field of 0.45 Tesla. The variation in line intensities of Ge plasma at different fluences of four spectral lines 561.63, 562.40, 589.39, and 648.31 nm in the presence and absence of the magnetic field is shown in Figure 3. It is revealed that emission intensities of all selected spectral lines are reduced at all fluences in the presence of the magnetic field.

3.1.2. Electron temperature

The Ge plasma genatrtedby laser is assumed to be in local thermodynamic equilibrium (LTE). In an LTE, the population of excited state follows the Boltzmann distribution. The electron temperature is calculated using the Boltzmann plot method, which is governed by the following relation (Harilal *et al.*, 1998*a*, *b*; Bashir *et al.*, 2012)

$$\ln\left(\frac{\lambda_{mn} I_{mn}}{g_m A_{mn}}\right) = -\frac{E_m}{KT_e} + \ln\left(\frac{N(T)}{U(T)}\right), \quad (1)$$

where E_m, T_e, k, $U(T)$, and $N(T)$ are the energy of upper state, electron temperature, Boltzmann constant, partition function, and total number density. On the left-hand side, λ_{mn}, I_{mn}, g_m, and A_{mn} are the wavelength, intensity, statistical weight, and transition probability, respectively. The plot of E versus $\ln(\lambda_{mn} I_{mn}/g_m A_{mn})$ gives a straight line whose slope is equal to $-1/KT_e$. From the slope of the graph the electron temperature is evaluated.

In the present work, four lines are selected for investigating the effect of the magnetic field on the excitation

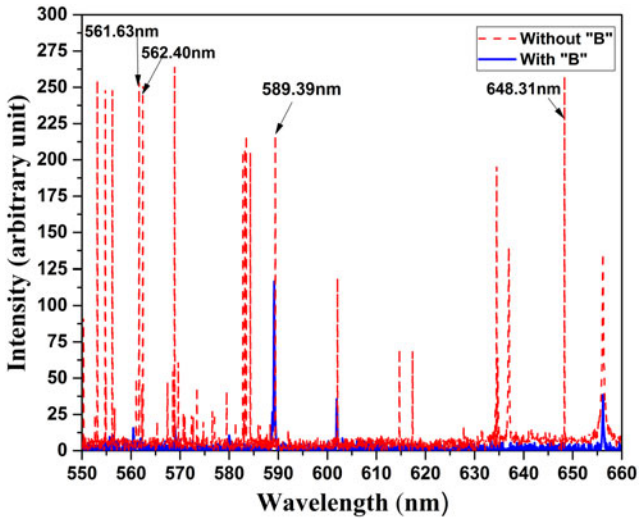

Fig. 2. The emission spectra of laser-induced Ge plasma in the absence and presence of the magnetic field under Ar environment at a pressure of 50 Torr and at a fluence of 16 J/cm^2.

https://doi.org/10.1017/S0263034617000039 Published online by Cambridge University Press

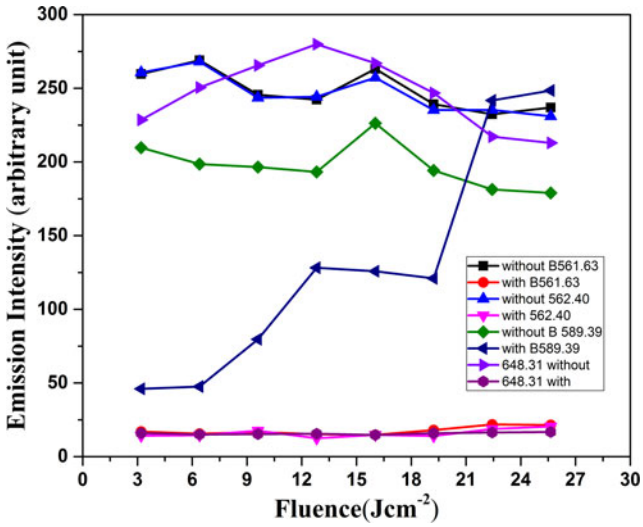

Fig. 3. The emission intensity of laser-produced Ge plasma in the absence and presence of the magnetic field at various fluences in Ar gas at pressure of 50 Torr.

temperature of laser-induced Ge plasma. The standard spectroscopic data such as statistical weight, transition probability, energy of upper state, and the Boltzmann constant are taken from the NIST database (NIST, 2005) and literature (Shakeel *et al.*, 2016), and are listed in Table 1. The variation of electron temperature as a function of laser fluence in the absence and presence of the magnetic field is shown in Figure 4. The values of electron temperature range from 15,269 to 16,190 K without the magnetic field, whereas this range enhances from 17,589 to 20,123 K with the magnetic field at various fluenc values .The graph shows that electron temperature increases with increasing fluence from 3.2 to 12.8 J/cm^2 and achieves its maxima at 12.8 J/cm^2. It decreases with further increase in fluence varying from 16 to 19.2 J/cm^2 and then it becomes saturated with further increasing fluence from 22 J/cm^2 to a maximum value 25.6 J/cm^2. It is observed from the graph that higher values of electron temperature are achieved in the presence of the magnetic field as compared with the absence of the magnetic field.

3.1.3. Electron number density

Another important parameter for the plasma characterization is number density. In order to determine the number density, spectroscopic method is used (Ley, 2014). Stark broadening profile is used to measure the number density, in which number density is related to the full-width at half-maximum (FWHM) of stark broadening lines. Spectral broadening with FWHM is given by the following expression (Harilal *et al.*, 1998*a*, *b*; Bashir *et al.*, 2012):

$$\Delta\lambda_{1/2} = 2\omega\left(\frac{N_e}{10^{16}}\right) + 3.5\hat{A}\left(\frac{N_e}{10^{16}}\right)^{1/4}\left(1 - 1.2N_D^{-1/3}\right)\omega\left(\frac{N_e}{10^{16}}\right), \quad (2)$$

Where $\Delta\lambda_{1/2}$, ω, N_e, $\hat{A}$, and N_D is the FWHM of spectral lines, electron impact width parameter, electron number density, and Debye shielding parameter, respectively. Debye shielding parameter is actually the number of particles in a Debye sphere, which can be calculated by using the following relation (Shaikh *et al.*, 2007).

$$N_D = 1.72 \times 10^9 \frac{T^{3/2\,(eV)}}{N_e^{1/2}(cm^{-3})}. \quad (3)$$

The first term in Eq. (2) refers to electron broadening and second term is ascribed to ion broadening. The second term is ignored due to minor contribution of ion broadening. Thus, Eq. (2) reduces to following relation (Bashir *et al.*, 2012).

$$\Delta\lambda_{1/2} = 2\omega\left(\frac{N_e}{10^{16}}\right). \quad (4)$$

The graph of Figure 5 shows the evaluated value of number density in the absence and presence of the magnetic field at various fluences. It reveals that with increasing laser fluence, electron number density increases. The maximum value of density is achieved at fluence of 12.8 J/cm^2. After achieving maxima, it decreases with further increasing fluence. The trend of the number density is same as observed in case of excitation temperature. The values of number density varies from 8.5×10^{17} to 1.3×10^{18} cm^{-3} without the magnetic field and from 1×10^{18} to 3.6×10^{18} cm^{-3} with the magnetic field. It is seen from the graph that higher values of electron density are achieved in the presence of a magnetic field as compared with the absence of magnetic field.

Table 1. *The relevant spectroscopic data of laser-produced Ge plasma taken from NIST Database (NIST) and literature (Shakeel* et al.*, 2016)*

Wavelength (nm)	Transitions	Energy of upper level E_m (cm^{-1})	Statistical weight g_m	Transitions probabilities (108 s^{-1})
561.63	$4s^2 4p5s \rightarrow 3P^o$	55,503.2026	1	0.042
562.40	$3P_o^o \rightarrow {}^1P_1$	55,235.8344	3	0.044
589.39	$5p2P^{3/2} \rightarrow 5s2S^{1/2}$	79,366.627	4	0.9144
648.31	$6s2S^{1/2} \rightarrow 5p2P^{3/2}$	94,784.529	2	0.8436

https://doi.org/10.1017/S0263034617000039 Published online by Cambridge University Press

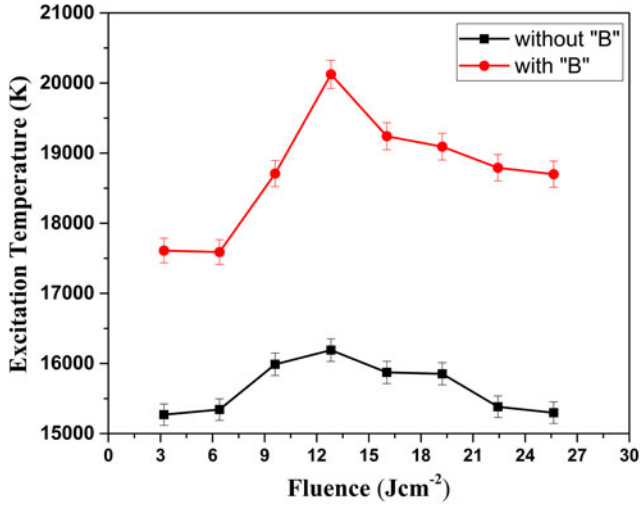

Fig. 4. The variation in excitation temperature of Ge plasma at various fluences in the absence and presence of the magnetic field under 50 Torr pressure of Ar gas.

4. DISCUSSION

LIBS analysis shows that emission intensity, electron temperature, and number density are strongly affected by the magnetic field. The reduction in the emission spectra is attributed to reduction in lifetime of upper state of Ge plasma due to confinement effect. When the magnetic field confines the plasma and free expansion of plasma is restricted, the interaction time for recombination is very much reduced (Shen *et al*., 2006). When confinement processes are enhanced then three body recombination overcomes radiative process and will be responsible to reduce the emission intensity in the presence of a magnetic field as compared with field-free region (Raju *et al*., 2014; Lan *et al*., 2015). Both excitation temperature and number density are higher in the presence of a magnetic field as compared with the absence of a magnetic field. The trends of both electron temperature and number density are divided into three main regions, the first one increasing, second one is decreasing and then there is a saturation regime. The initial increase in excitation temperature and number density, with increasing fluence is due to more energy deposition and corresponding enhanced excitation and deexcitation of Ge plasma as well as the increased ablation rate (Harilal *et al*., 2004). Two main phenomenon, that is, inverse bremsstrahlung ionization (IBI) and multi photon ionization (MPI) are responsible for the laser energy absorption by a Ge target for plasma formation. These both processes are responsible for generation and growth of electrons (Harilal *et al*., 1998*a*, *b*). With increasing laser fluences both processes of MPI and IBI increase and correspondingly the energy and density of generated electrons are increased. When density of plasma becomes equal to greater than the critical density (Joshi *et al*., 2010).

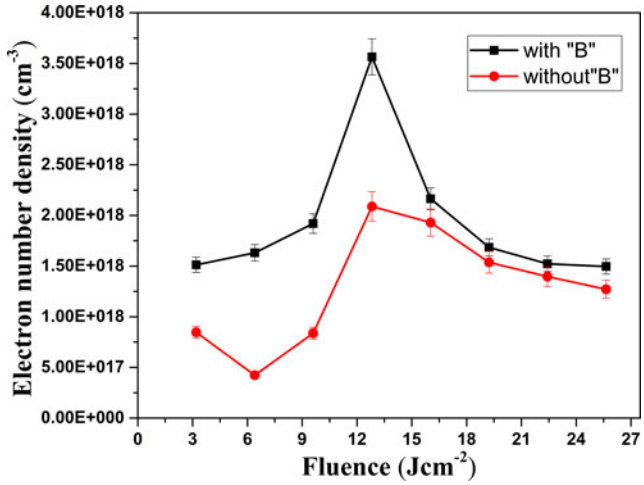

Fig. 5. The variation in the number density of Ge plasma at various fluences in the absence and presence of magnetic field under 50 Torr pressure of Ar gas.

$$n_e = \frac{10^{21}}{\lambda} = 9.5 \times 10^8 \text{ m}^{-3}. \quad (5)$$

Plasma frequency becomes equal to the frequency of laser light and due to resonance phenomenon plasma absorbs increasing electromagnetic radiations and shielding effect occur. This shielding is responsible to reduce the energy absorption by the target surface (Miziolek *et al*., 2006) and consequently excitation temperature and number density is reduced. The insignificant variations in both T_e and N_e, at higher fluences are attributed to self-regulated regimes (Radziemski & Cremers, 2006). Three mechanisms, that is, elastic collision, electron heating due to collisional deexcitation of metastable ions, and recombination of ions are responsible for the variation of excitation temperature (Harilal *et al*., 1998*a*, *b*).

Both the excitation temperature and number density in the presence of the magnetic field are greater than the absence of the magnetic field, because the magnetic field affects the ablated species of plasma. Several additional phenomenon are introduced, that is, plume confinement, conversion of kinetic energy into plasma thermal energy, ion acceleration, and plasma instabilitis (Joshi *et al*., 2010). Without magnetic field the plasma expands freely. When a magnetic field is applied it introduces a resistive Lorentz force on the plasma species and slows down the propagation of ablated plume. Plasma is not fully stopped by the applied magnetic field rather than plume penetrates into the magnetic field and propagates slowly. The expansion of plume is normal to the magnetic field (Harilal *et al*., 2004). For understanding of our experiemntal results, plasma parameter β is introduced, which is the ratio between plasma particle pressure and magnetic pressure. From magnetohydronamic (MHD) equation β is given by (Shen *et al*., 2006).

$$\beta = \frac{8\pi n_e k T_e}{B^2} = \frac{\text{Plasma pressure}}{\text{Magnetic pressure}}, \quad (6)$$

https://doi.org/10.1017/S0263034617000039 Published online by Cambridge University Press

where n_e, k, and T_e are the number density, Boltzmann constant, and electron temperature, respectively, and B is the magnetic field strength. β is the ratio of plasma pressure to magnetic pressure, it is dimensionless quantity and it shows the diamagnetic effect (Rai *et al*., 1998, 1999).

$$\frac{v_2}{v_1} = \left(1 - \frac{1}{\beta}\right)^{1/2}, \tag{7}$$

where v_1 and v_2 are the asymptotic plasma expansion velocity in the absence and presence of a magnetic field, respectively (Shen *et al*., 2006). When $\beta = 1$, thermal pressure becomes equal to magnetic pressure, plasma will be stopped by the magnetic field. The magnetic confinement will be effective for $\beta < 1$. The magnetic confinement does not remain effective for $\beta > 1$. Using Eq. (6) the value of β is calculated for the maximum and minimum value of electron temperature and number density. The calculated values of β is <1 for all the cases and are tabulated in Table 2, which shows the existence of plume magnetic confinement. Our measurements show that we can treat our plasma as a compressible fluid (Lan *et al*., 2015).

The enhancement in electron temperature in the presence of a magnetic field relative to the field-free case is due to the two effects: the adiabatic compression and Joule heating effect by the magnetic field (Harilal *et al*., 2004). Joule heating can be realized by considering a MHD model to trace the expansion of the ionized plume in a magnetic sphere. According to the MHD model, the generalized form of Ohm's law is given as (Boyd & Sanderson, 2003)

$$E + V \times B = J/\sigma_0 + (J \times B)/n_e e, \tag{8}$$

where on the left-hand side of the above equation E, B, and V are the electric field, magnetic field, and mass flow velocity, respectively. On the right-hand side J, σ_0, n_e, and e are electron conduction current, conductivity, electron density, and charge of electron, respectively. When the expansion of plasma takes place across the magnetic field, heating can occur due to the energy gained by the electrons from the plume kinetic energy and the work is executed against the $J \times B$ term that acts to slow the flow. The $J \times B$ force acts to push the plasma until the magnetic pressure is balanced by the plasma pressure. This will lead to Joule heating of the electrons, so that electrons can continue to excite higher-charge states (Harilal *et al*., 2004). Magnetic field promotes the electron collisional excitation, which leads to increase the electron temperature and number density.

Electron density in the presence of a 0.45 Tesla magnetic field is higher as compared with the absence of the magnetic field. Because when a magnetic field is applied plasma decelerates in the backward direction and confines itself. As a result number density increases. In the presence of a magnetic field, velocity and expansion of plasma decrease and the density increases compared with the absence of a magnetic field (Neogi & Thareja, 1999).

4.1. Magnetic field effect on surface modifications of laser-irradiated Ge

SEM micrographs of Figure 6 show the overall ablated area of Ge in the absence of the magnetic field under Ar environment irradiated by 50 shots of Nd: YAG laser at wavelength of 1064 nm and repetition rate of 10 Hz at different fluences of (a) 6.4, (b) 12.8, (c) 19.2, and (d) 25.6 J/cm^2 . Elliptical-shaped craters are formed by laser irradiation. The area of irradiated craters in the absence of a magnetic field at the fluence of 6.4, 12.8, 19.2, and 25.6 J/cm^2 are 0.28×10^{-6}, 0.47×10^{-6}, 0.55×10^{-6}, and 0.45×10^{-6} cm^2, respectively. In the central ablated region, no surface structures are formed. It can be attributable to maximum energy deposition at the center. However, at the peripheries, indistinct rims are formed, whose magnified views are shown in Figure 7. The surface of peripheral ablated region is mainly characterized by the formation of cones, cavities, and droplets. For the lowest fluence of 6.4 J/cm^2, non-uniform cones and cavities are observed as shown in 7(a). The cones are formed when the pressure of incoming laser irradiation causes depression as well as stresses on the target surface. When laser pulse is over, relaxation of these stresses causes the evolution of cones (Mansour *et al*., 2006). Cavity formation is attributable to the recoil pressure of plasma that exceeds the surrounding pressure and the molten material can be expelled out explosively from the target (Körner *et al*., 1996). Contaminations, inclusions, and small pits are responsible for different size of cavities (Barmina *et al*., 2009). As shown in Figure 7b, the cone height decreases and the density increases with increasing laser fluence. Unorganized and self-organized droplets are also seen. The enhanced energy deposition is responsible to detach the material in the form of droplets. Droplet

Table 2. *The evaluated values of plasma parameter β for all different calculated values of electron temperature and number density of Ge plasma, in the presence of Ar at pressure of 50 Torr at different laser fluences*

Fluence (J/cm^2)	3.2	6.4	9.6	12.8	16	19.2	22	25.6
T_e (K)	17,610	17,589	18,708	20,123	19,242	19,092	18,792	18,700
n_e (cm^{-3})	1.5×10^{18}	1.6×10^{18}	1.9×10^{18}	3.6×10^{18}	2.2×10^{18}	1.7×10^{18}	1.5×10^{18}	1.4×10^{18}
β	0.0452	0.0481	0.0608	0.1239	0.0724	0.055	0.0482	0.0447

https://doi.org/10.1017/S0263034617000039 Published online by Cambridge University Press

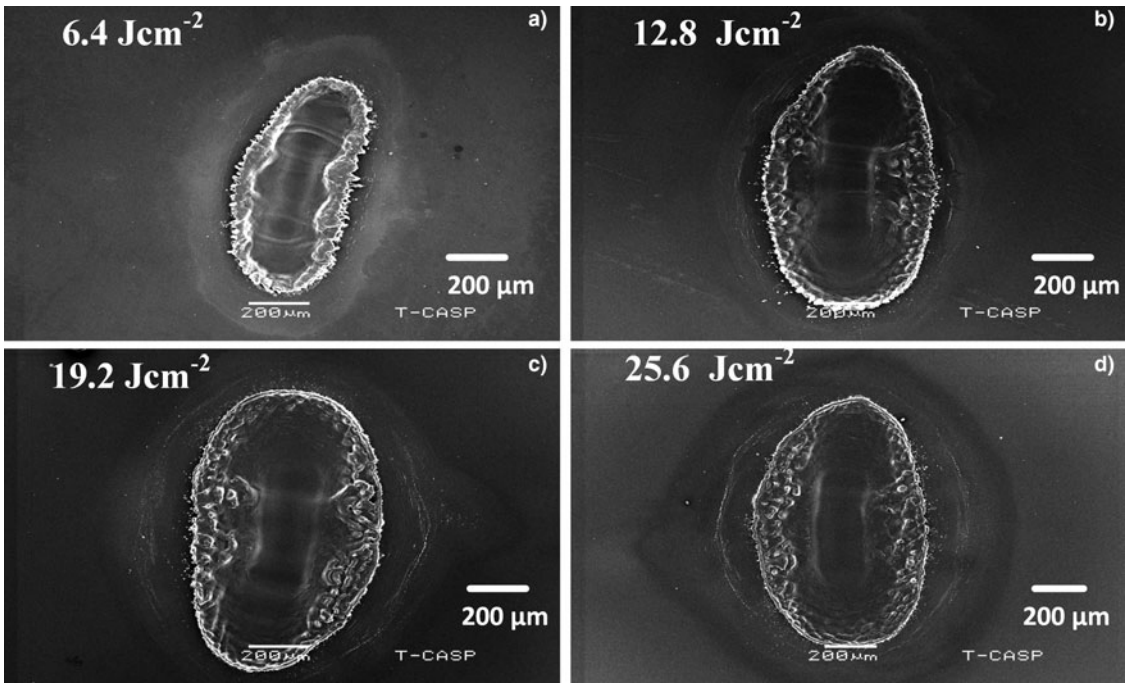

Fig. 6. SEM images revealing the overall ablated area of Ge in the absence of the magnetic field at different fluences of (a) 6.4 J/cm^2, (b) 12.8 J/cm^2, (c) 19.2 J/cm^2, and (d) 25.6 J/cm^2.

formation can be attributed due to hydrodynamic instability, which largely depends upon laser irradiance and material properties (Bleiner & Bogaerts, 2006). Depending upon absorption coefficient (59%) and thermal diffusivity of material, volumetric heating occurs during laser target interaction. During heating and vaporization, a temperature gradient is generated, which leads to the expansion of molten material that can be considered a possible reason for droplet formation (Bleiner & Bogaerts, 2006). Figure 7c depicts that non-uniform melting and indistinct features are formed at a

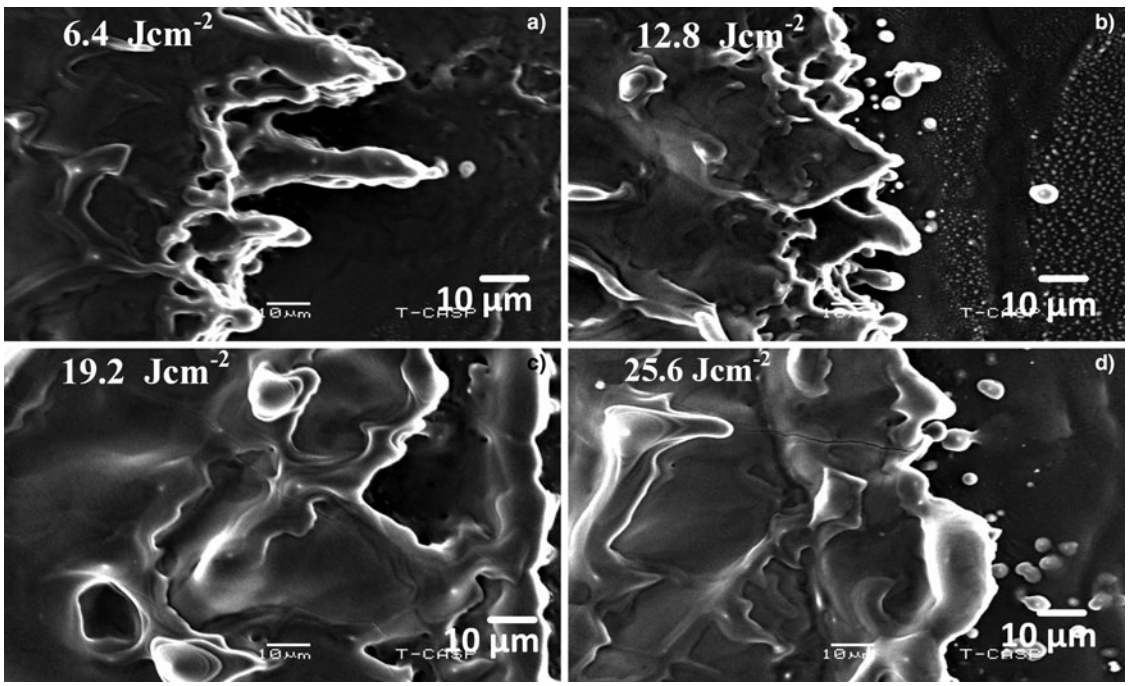

Fig. 7. SEM images revealing the peripheral ablated area of Ge in the absence of the magnetic field at a fluence of (a) 6.4 J/cm^2, (b) 12.8 J/cm^2, (c) 19.2 J/cm^2, and (d) 25.6 J/cm^2.

https://doi.org/10.1017/S0263034617000039 Published online by Cambridge University Press

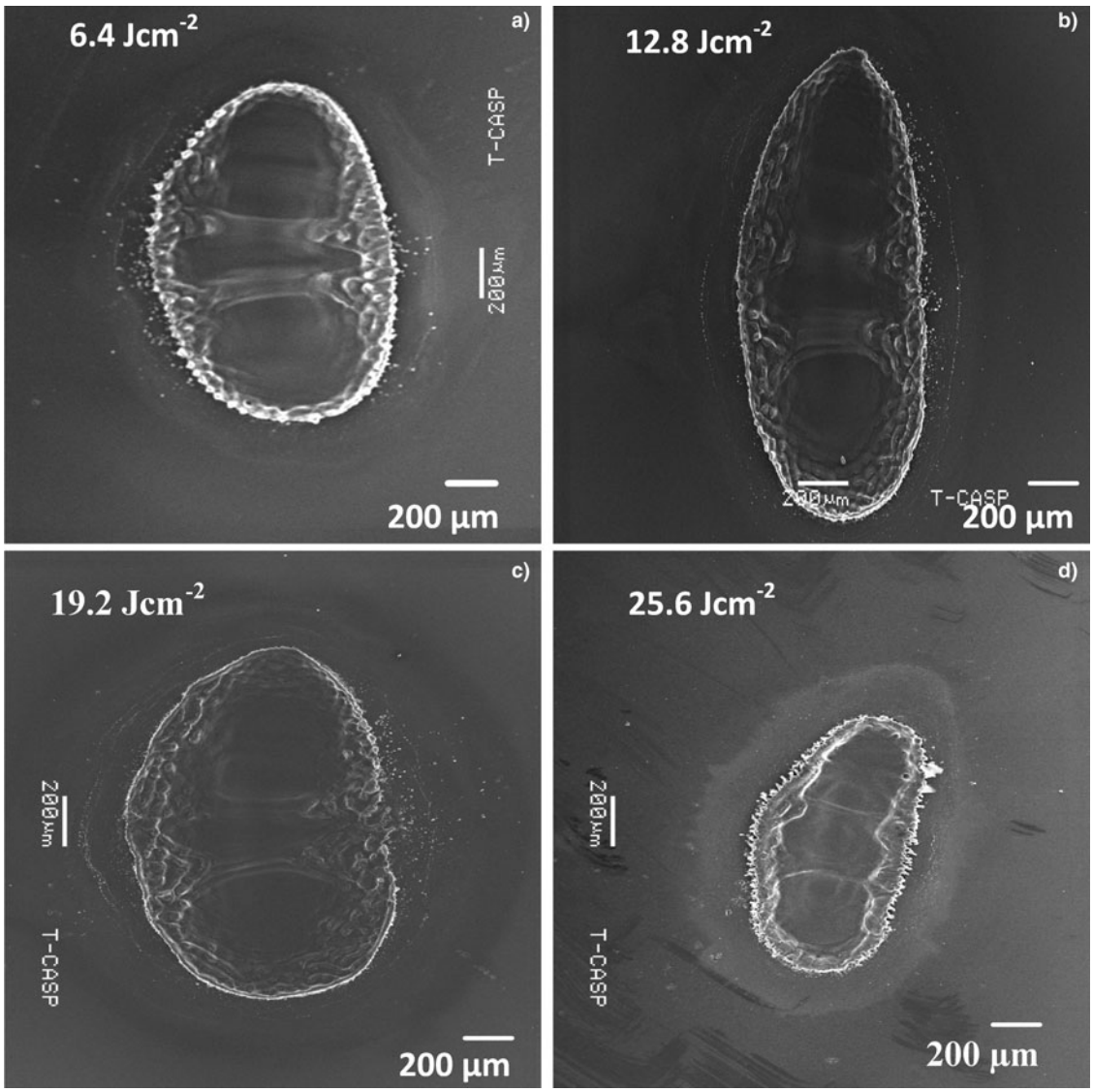

Fig. 8. SEM images revealing the overall ablated area of Ge in the presence of the magnetic field at different fluences of (a) 6.4 J/cm^2, (b) 12.8 J/cm^2, (c) 19.2 J/cm^2, and (d) 25.6 J/cm^2.

fluence of 19.2 J/cm^2. Figure 7d illustrates that cones and cavities are vanished and only droplets are seen.

SEM micrographs of Figure 8 show the overall ablated area of Ge in the presence of the magnetic field at different fluences of (a) 6.4, (b) 12.8, (c) 19.2, and (d) 25.6 J/cm^2. Elliptical-shaped craters are formed by laser irradiation whose areas are 0.85×10^{-6}, 0.86×10^{-6}, 0.92×10^{-6}, and 0.49×10^{-6} cm^2, respectively. The irradiated areas are enhanced in the presence of a magnetic field as compared with field-free case, which is attributed to more energy deposition by laser and cofined plasma-induced plasma effects on Ge taget. At the peripheries distinct rims are formed, whose magnified views are shown in Figure 9. Droplets, ridges, cavities, and cones are the dominant features at the peripheral ablated areas for all fluences. At a fluence of 6.4 J/cm^2, wave-like ridges and droplets are formed as shown in Figure 9a. The formation of ridges depends on recoil pressure and laser fluence. With the increase in laser fluence the width of plasma plume increases. When the pressure of the plasma is higher than the surrounding pressure, the liquefied material is expelled explosively from the irradiated surface due to the violent recoil pressure and becomes a possible cause for wave-like ridges (Yu & Lu, 1999). With increasing laser fluence waves-like ridges become less pronounced and more diffusive. Figure 9b shows the surface modification of Ge at a fluence of 12.8 J/cm^2. The formation of large-sized droplets and ridges is seen. Figure 9c illustrates the surface modifications of Ge at a fluence of 19.2 J/cm^2 with the appearance of cavities and cones. Droplets disappear beacause all energy is utilized in cavities formation. Figure 9d depicts the formation of large number of cone at a fluence of 25.6 J/cm^2. With increasing fluence cavities are vanished and cones

https://doi.org/10.1017/S0263034617000039 Published online by Cambridge University Press

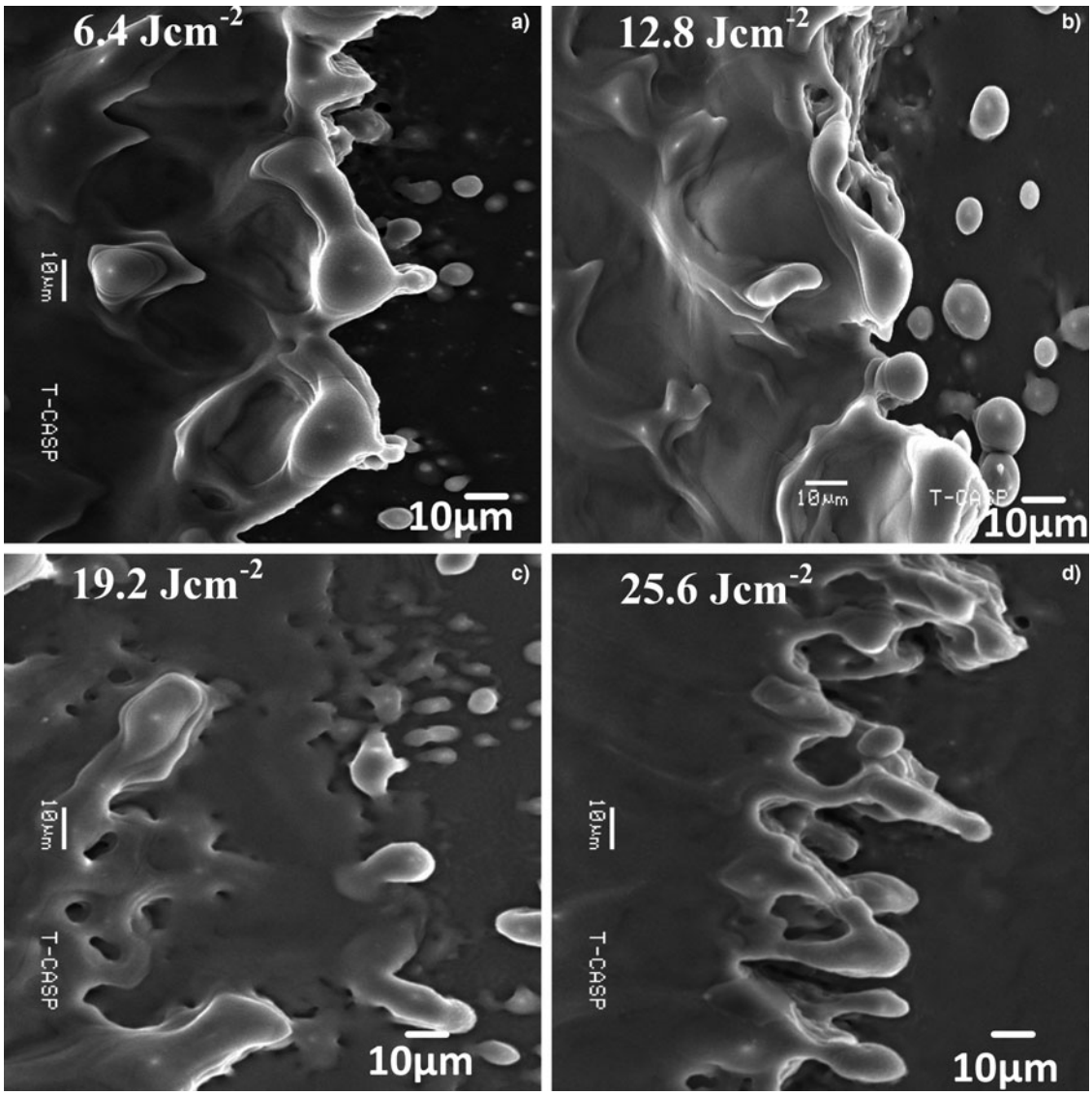

Fig. 9. SEM images revealing the peripheral ablated area of Ge in the presence of the magnetic field. (a) 6.4 J/cm^2, (b) 12.8 J/cm^2, (c) 19.2 J/cm^2, and (d) 25.6 J/cm^2.

become more pronounced. The disappearance of cavities at higher fluence is due to refilling of the molten material. The ablation of Ge in the case of Ar is responsible for the growth of more distinct features due to more energy deposition. In the absence of the magnetic field, indistinct features with non-uniform melting are observed, whereas, in the presence of the magnetic field distnict features with distnict rims and uniform melting are observed.

Area of irradiated spot in the presence of the magnetic field is higher as compared with absence of a magnetic field due to more energy deposition of confined plasma. The higher excitation temperature provides more energy to the lattice and correspondingly the surface modifications in the form of large-sized craters are clearly observed. LIBS analysis is well correlated with SEM modification of Ge after laser irradiation.

5. CONCLUSIONS

It is found that the transverse magnetic field significantly influences plasma temperature, density, and surface morphology of Ge. There is significant enhancement in excitation temperature and number density of Ge plasma in the presence of the magnetic field as compared with the absence of a magnetic field. Both plasma parameters are also strongly dependent upon the fluence. With increasing fluence, they increase, achieve their maxima, and then decrease. This trend remains same for Ge plasma observed in the presence of the magnetic field as well as for field free case. At a fluence of 12.8 J/cm^2, the maxima of both plasma parameters (T_e, n_e) are obtained. The value of excitation temperature varies from 15,269 to 16,190 K in the absence of the magnetic field. This range increases from 17,589 to 20,123 K in the presence of a

https://doi.org/10.1017/S0263034617000039 Published online by Cambridge University Press

magnetic field. Similarly the electron number density varies from 8.5×10^{17} to 1.3×10^{18} cm^{-3} in the field-free case and its range increases from 1.5×10^{18} to 1.4×10^{18} cm^{-3} in the presence of a magnetic field. Plasma confinement in the presence of magnetic filed is confirmed by the calculated value of β, which is smaller than 1 for all cases. Non-uniform melting and indistinct structures are observed in the absence of the magnetic field. Distinct and well-defined structuring is observed in the presence of the magnetic field. Therefore the magnetic field can be used for clean abation as well as for the growth of well-defined structures. These structures can enhance electrical, optical, and field emission properties of Ge. By controlling plasma parameters under different conditions of laser fluences and magnetic field employment the surface structuring of materials can be controlled in a better way. Magnetic field can enhance the plasma parameters and hence can make it more useful for thin-film deposition, ion implantation, and micro/nanostructuring of materials.

ACKNOWLEDGMENTS

We are thankful to Higher Education Commission (HEC) of Pakistan for funding the project "Strengthening of laser facilities" at Centre for Advanced Studies in Physics (CASP), Government College University (GCU) Lahore". We are also thankful to Director CASP Prof. Dr. Riaz Ahmad and Dr. Tousif Hussian from CASP for providing SEM and other facilities.

REFERENCES

Ahmad, S., Bashir, S., Ali, N., Yousaf, D., Naeem, A., Ahmad, R. & Khaleeq-ur-Rahman, M. (2014). Effect of ion irradiation on the surface, structural and mechanical properties of brass. *Nucl. Instrum. Methods B* **325**, 5.

Arshad, A., Bashir, S., Hayat, A., Akram, M., Khalid, A., Yaseen, N. & Ahmad, Q. S. (2016). Effect of magnetic field on laser-induced breakdown spectroscopy of graphite plasma. *Appl. Phys. B* **122**, 1.

Barmina, E.V., Barberoglu, M., Zorba, V., Simakin, A.V., Strakis, E., Fotakis, K. & Shafeev, G.A. (2009). Surface nanotexturing of tantalum by laser ablation in water. *Quant. Electron.* **39**, 89.

Bashir, S., Farid, N., Mahmood, K. & Rafique, M.S. (2012). Influence of ambient gas and its pressure on the laser-induced breakdown spectroscopy and the surface morphology of laser-ablated Cd. *Appl. Phys. A* **107**, 203.

Behera, N., Singh, R. & Kumar, A. (2015). Confinement and re-expansion of laser induced plasma in transverse magnetic field: Dynamical behaviour and geometrical aspect of expanding plume. *Phys. Lett. A* **379**, 2215.

Bleiner, D. & Bogaerts, A. (2006). Multiplicity and contiguity of ablation mechanisms in laser-assisted analytical micro-sampling. *Spectrochim. Acta B* **61**, 421.

Boyd, T.J.M. & Sanderson, J.J. (2003). *The Physics of Plasmas*. UK: Cambridge Unversity Press.

Burger, M., Pantic, D., Nikolic, Z. & Djenize, S. (2016). Shielding effects in the laser-generated copper plasma under reduced pressures of He atmosphere. *J. Quant. Spectrosc. Radiat. Transfer* **170**, 19.

El-Saeid, R., Abdelhamid, M. & Harith, M. (2016). Laser-induced breakdown spectroscopy on metallic samples at very low temperature in different ambient gas pressures. *Spectrochim. Acta B* **116**, 1.

Farid, N., Bashir, S. & Mahmood, K. (2011). Effect of ambient gas conditions on laser-induced copper plasma and surface morphology. *Phys. Scr.* **85**, 015702.

Guo, L., Hu, W., Zhang, B., He, X., Li, C., Zhou, Y., Cai, Z., Zeng, X. & Lu, Y. (2011). Enhancement of optical emission from laser-induced plasmas by combined spatial and magnetic confinement. *Opt. Exp.* **19**, 14067.

Hahn, D. & Lunden, M. (2000). Aerosol science & technology. *Aerosol Sci. Technol.* **33**, 30.

Harilal, S., Bindhu, C., Nampoori, V. & Vallabhan, C. (1998*a*). Influence of ambient gas on the temperature and density of laser produced carbon plasma. *Appl. Phys. Lett.* **72**, 167.

Harilal, S., Bindhu, C., Nampoori, V. & Vallabhan, C. (1998*b*). Temporal and spatial behavior of electron density and temperature in a laser-produced plasma from $YBa_2Cu_3O_7$. *Appl. Spectrosc.* **52**, 449.

Harilal, S., Tillack, M., O'shay, B., Bindhu, C. & Najmabadi, F. (2004). Confinement and dynamics of laser-produced plasma expanding across a transverse magnetic field. *Phys. Rev. E* **69**, 026413.

Joshi, H., Kumar, A., Singh, R. & Prahlad, V. (2010). Effect of a transverse magnetic field on the plume emission in laser-produced plasma: An atomic analysis. *Spectrochim. Acta B* **65**, 415.

Körner, C., Mayerhofer, R., Hartmann, M. & Bergmann, H. (1996). Physical and material aspects in using visible laser pulses of nanosecond duration for ablation. *Appl. Phys. A* **63**, 123.

Lan, H., Wang, X., Chen, H., Zou, D. & Lu, P. (2015). Influence of a magnetic field on laser-produced Sn plasma. *Plasma Sourc. Sci. Technol.* **24**, 055012.

Ley, H.-H. (2014). Analytical methods in plasma diagnostic by optical emission spectroscopy: A tutorial review. *J. Sci. Technol.* **6**, 49.

Mansour, N., Jamshidi-Ghaleh, K. & Ashkenasi, D. (2006). Formation of conical microstructures of silicon with picosecond laser pulses in air. *J. Laser Micro/Nanoeng.* **1**, 12.

Michel, A.P., Lawrence-Snyder, M., Angel, S.M. & Chave, A.D. (2007). Laser-induced breakdown spectroscopy of bulk aqueous solutions at oceanic pressures: Evaluation of key measurement parameters. *Appl. Opt.* **46**, 2507.

Miziolek, A.W., Palleschi, V. & Schechter, I. (2006). *Laser Induced Breakdown Spectroscopy*. UK: Cambridge University Press.

Neogi, A. & Thareja, R. (1999). Dynamics of laser produced carbon plasma expanding in a nonuniform magnetic field. *J. Appl. Phys.* **85**, 1131.

NIST, National Institute of Standard and Technology (2005). http://physics.nist.gov/asd.

Pisarczyc, T. & Kasperczuk, A. (1999). Measurement of electron density in plasma disturbed by strong transverse magnetic field. *Laser Part. Beams* **17**, 313.

Radziemski, L.J. & Cremers, D.A. (2006). *Handbook of Laser Induced Breakdown Spectroscopy (West Sussex)*. England: John Wiley & Sons.

Rafique, M.S., Khaleeq-Ur-Rahman, M., Riaz, I., Jalil, R. & Farid, N. (2008). External magnetic field effect on plume

https://doi.org/10.1017/S0263034617000039 Published online by Cambridge University Press

images and X-ray emission from a nanosecond laser produced plasma. *Laser Part. Beams* **26**, 217.

Rai, V.N., Jagdish, P.S., Fang, Y.Y. & Robert, L.C. (2003*a*). Study of optical emission from laser-produced plasma expanding across an external magnetic field. *Laser Part. Beams* **21**, 65.

Rai, V.N., Shukla, M. & Pant, H. (1999). An X-ray biplanar photodiode and the X-ray emission from magnetically confined laser produced plasma. *Pramana J. Phys*. **52**, 49.

Rai, V.N., Shukla, M. & Pant, H.C. (1998). Some studies on picosecond laser-produced plasma expanding across uniform external magnetic fields. *Laser Part. Beams* **16**, 431.

Rai, V.N., Zhang, H., Yueh, F.Y., Singh, J.P. & Kumar, A. (2003*b*). Effect of steady magnetic field on laser-induced breakdown spectroscopy. *Appl. Opt*. **42**, 3662.

Raju, M.S., Singh, R., Gopinath, P. & Kumar, A. (2014). Influence of magnetic field on laser-produced barium plasmas: Spectral and dynamic behaviour of neutral and ionic species. *J. Appl. Phys*. **116**, 153301.

Roy, A., Harilal, S.S., Hassan, S.M., Endo, A., Mocek, T. & Hassanein, A. (2015). Collimation of laser-produced plasmas using axial magnetic field. *Laser Part. Beams* **33**, 175.

Shaikh, N.M., Hafeez, S. & Baig, M.A. (2007). Comparison of zinc and cadmium plasma parameters produced by laser-ablation. *Spectrochim. Acta B* **62**, 1311.

Shakeel, H., Arshad, S., Haq, S. & Nadeem, A. (2016). Electron temperature and density measurements of laser induced germanium plasma. *Phys. Plasmas* **23**, 053504.

Shen, X., Lu, Y., Gebre, T., Ling, H. & Han, Y. (2006). Optical emission in magnetically confined laser-induced breakdown spectroscopy. *J. Appl. Phys*. **100**, 053303.

Yu, J. & Lu, Y. (1999). Laser-induced ripple structures on Ni–P substrates. *Appl. Surf. Sci*. **148**, 248.

https://doi.org/10.1017/S0263034617000039 Published online by Cambridge University Press